

STRUCTURAL CHARACTERIZATION OF THE INTERFACIAL SELF-ASSEMBLY OF POLYELECTROLYTES

Supplimentary informations

by R Chachanidze *et al.*

I. INTERFACIAL RHEOMETRY

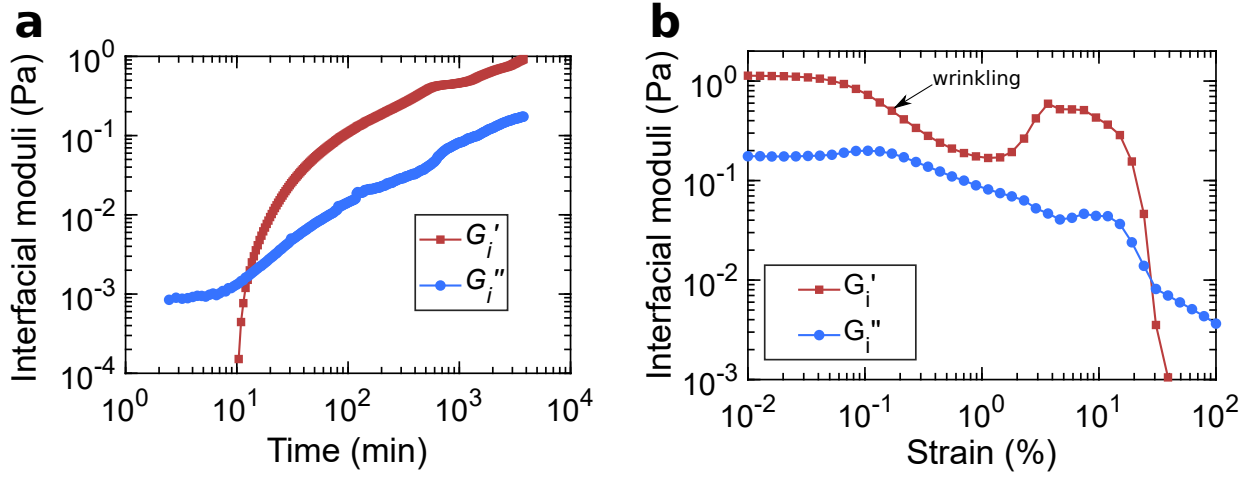


Figure 1: **a:** We performed a long term membrane formation for a single case (0.1% w/w chitosan, 0.1% w/w PFacid , $f = 0.5$ Hz, $\gamma = 0.03\%$) in order to perform a strain sweep on a thick membrane and define the limits of linear elastic regime. **B:** We observed that for long term formed membranes (>24 hours) the linear elastic regime was limited to surprisingly low values of strain (<0.1 %). The direct microscopic observation of the membrane decorated with tracing particles during the strain sweep experiments showed that this highly non-linear behaviour was caused by wrinkling instability of the membrane. The deformation of ≈ 20 % lead to the rapid decline in G'_i . The direct observation showed that it was caused by the loss of connectivity between the membrane and the bicone.

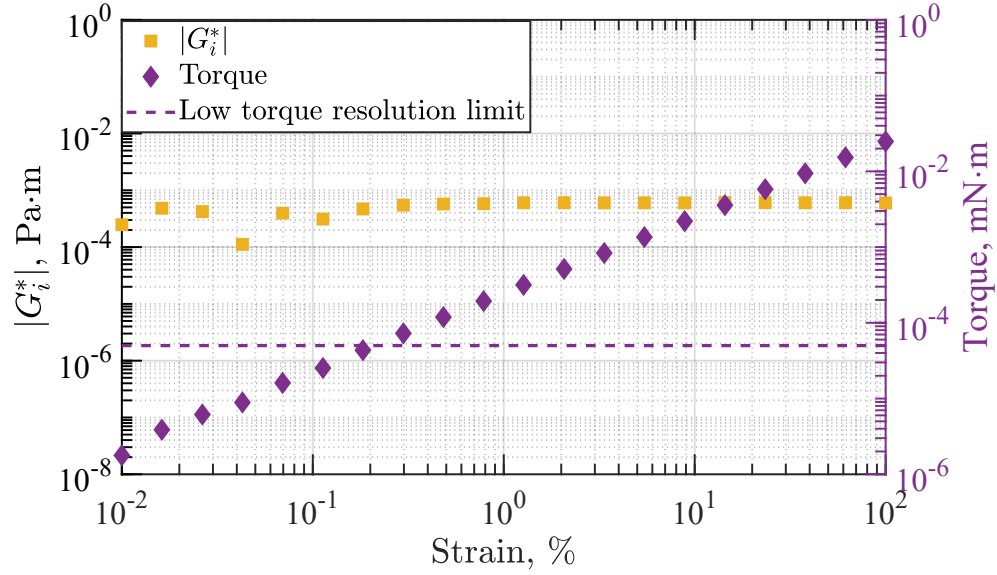


Figure 2: Strain sweep of the chitosan/oil interface. The test was performed with the bicone geometry ($f = 0.5$ Hz). The aqueous phase contained 0.1% w/w chitosan. PFacid was not added to the oil phase. The result illustrates the steady state chitosan/oil interface without the complexation. **Note:** while the stable values of interfacial viscoelastic modulus G_i^* are obtained, without the solid membrane forming at the interface the Boussinesq number is very low ($Bo=0.242$ in this case). Thus this result is qualitative and served as a reference line.

II. DYNAMIC LIGHT SCATTERING

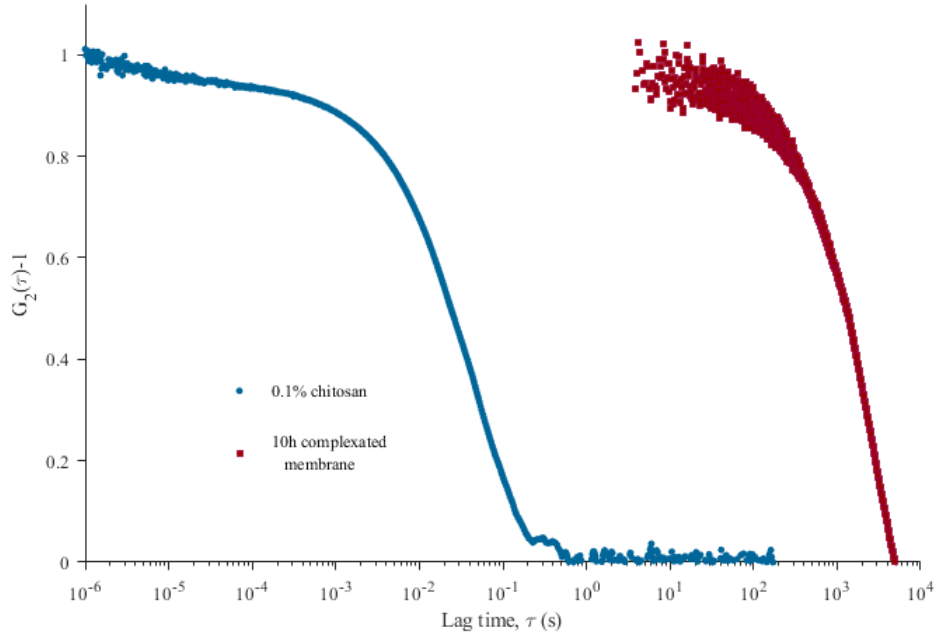


Figure 3: Two distinct cases demonstrating the changes in chitosan/PFAcid membrane DLS signature. The average characteristic relaxation time of chitosan solution (0.1% w/w) was $\tau = 0.88$ s. The relaxation time of fully formed membrane after 10 hours of complexation was 3488.4 s. Note, that DLS signature of the chitosan solution, being a fast process, was acquired using the PM as a receiver, while the DLS signature of the membrane was acquired with fast camera.

III. ATOMIC FORCE MICROSCOPY

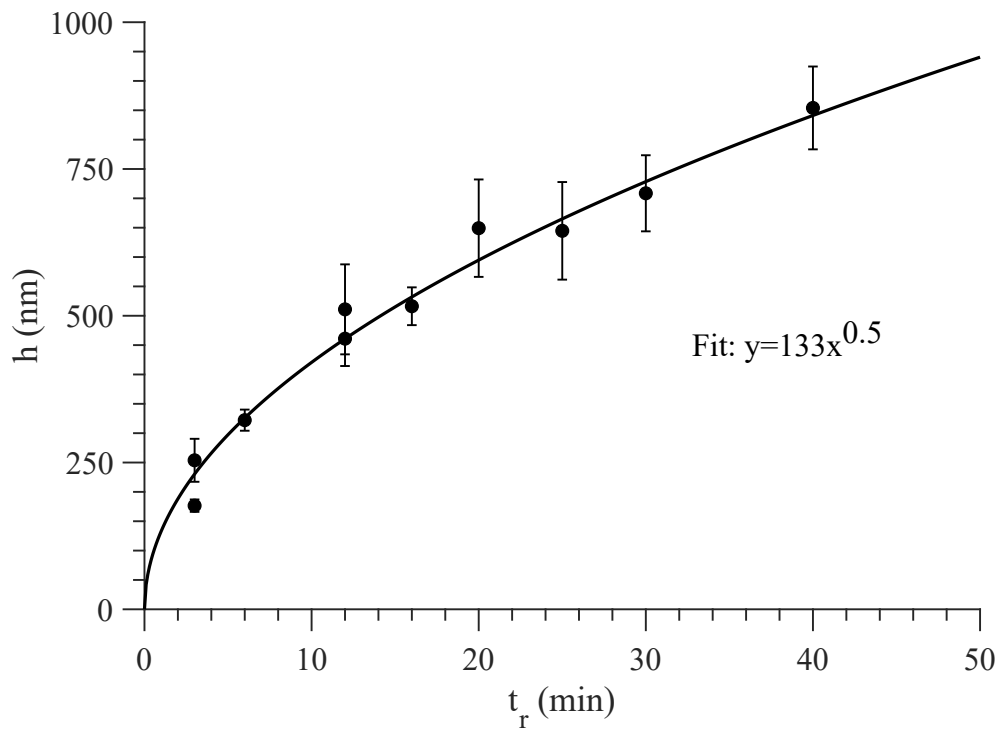
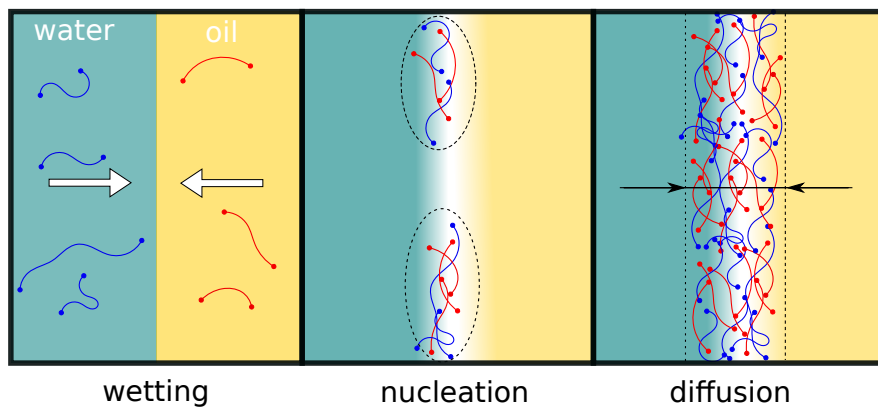


Figure 4

Graphical Abstract

Structural characterization of the interfacial self-assembly of polyelectrolytes

Revaz Chachanidze, Kaili Xie, Hanna Massaad, Denis Roux, Marc Leonetti, Clément de Loubens



Structural characterization of the interfacial self-assembly of polyelectrolytes

Revaz Chachanidze^{a,*}, Kaili Xie^{a,b}, Hanna Massaad^a, Denis Roux^a, Marc Leonetti^{a,c} and Clément de Loubens^a

^aUniv. Grenoble Alpes, CNRS, Grenoble INP, LRP, 38000 Grenoble, France

^bUniv. Bordeaux, CNRS LOMA UMR 5798, Talence F-33405, France

^cUniv. Aix-Marseille, CNRS, CINaM, Marseille, France

ARTICLE INFO

Keywords:
membrane
interface
rheology
dynamic light scattering

ABSTRACT

Controlling the assembly of colloids at liquid-liquid interfaces offers new ways to fabricate soft materials with specific physical properties. However, little is known of the relationships between the kinetics of interfacial assembly, structural and rheological properties of such interfaces. We studied the kinetics of the assembly of two oppositely charged polyelectrolytes using a multi-scale approach. Soft interfaces were formed from the complexation at water-oil interface of chitosan, a polysaccharide carrying positively charged groups, and a fatty acid exhibiting negative charges. The growth kinetics of the membrane was followed by interfacial rheometry and space- and time- resolved dynamic light scattering. This set of techniques revealed that the interfacial complexation was a multi-step process. At short time-scale, the interface was fluid and made of heterogeneous patches. At a ‘gelation’ time, the surface elastic modulus and the correlation between speckles increased sharply meaning that the patches percolated. Confocal and electron microscopy confirmed this picture, and revealed that the basic brick of the membrane was sub-micrometric aggregates of polyelectrolytes.

1. Introduction

Since pioneering observations by Ramsden [1] and Pickering [2] regarding the stabilization of emulsions and foams by colloidal particles trapped at interface, the interfacial assembly of colloids has seen growing interest from scientific communities. It opens the way to the fabrication of materials with specific physical properties such as films, capsules or structured liquids by using interfaces as scaffolds [3] as well as understanding some physiological functions [4]. These materials can be produced by droplet formation [5] or 3D-printing of liquid-liquid interfaces [6]. The main driving mechanism behind the self-assembly of colloids at interface is the process of minimization of interfacial energy, which can be tuned by an external stimulus [7] or by controlling the interactions between the particles [8]. As a result of this assembly, the interface can have a solid-like or liquid-like behaviour. One striking example is the possibility to design mechanically pH-responsive and self-healing microcapsules by interfacial assembly of polymer-polymer coacervates [9], which open the way to *in-situ* reconfigurable structured liquid interfaces.

Building materials based on interfacial assembly of colloids with tuneable properties (e.g. microencapsulation) requires understanding the interplay between the properties of the colloids, the kinetics of interfacial assembly and the resulting properties. For interfaces covered by model nanoparticles [10], the structure of the interface changes with the increasing surface coverage, from a fractal network of aggregates to a heterogeneous structure with voids, to a gel with dense clusters and eventually a densely-packed system [11, 12]. Consequently, viscoelasticity and yield points of these interfaces are controlled by the surface coverage, interparticle interactions and external field forces [12, 13].

H-bond acceptor and donor polymers have also been used to cover water-oil interfaces by interfacial complexation of both polymers [9]. For these systems, the elasticity is controlled by the type and strength of physical interactions [14]. Dupré de Baubigny *et al.* [15] investigated the kinetics of membrane growth on long time scales (> 1,000 s) and identified a diffusion limited process. However, the authors were surprised to observe that the process was faster when polymer molar mass increased. They related this observation to the description of the structure of the membrane as a gel-like porous network, with a pore size much smaller than the radius of the diffusing polymer chains. As a result, the diffusion process should be hindered by the entropic barrier. Another possible approach stabilising interfaces

*Corresponding authors: revaz.chachanidze@univ-grenoble-alpes.fr
ORCID(s): 0000-0002-4988-9168 (Clément de Loubens)

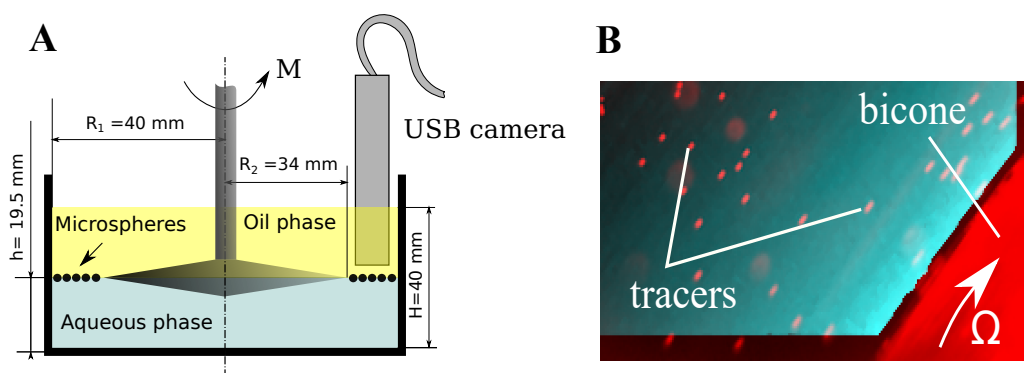


Figure 1: Interfacial rheometry by means of IRS. (A) Schematic representation of the bicone rheological cell used to probe the interfacial properties of chitosan / PFacid membrane. The interface was seeded with microparticles to visualize the velocity field of the interface with an immersed camera. (B) PTV at the water-oil interface, the color gradient shows the average velocity of tracers decreasing further when moving away from bicone.

25 is via formation of an interfacial complex whereby two oppositely charged polyelectrolytes are dissolved in different
 26 immiscible phases. [16, 17, 18, 19, 20, 21]. Upon contact, polycations and polyanions diffuse spontaneously towards
 27 the interface and form a membrane or a coacervate by electrostatic interactions. As for polymer-polymer interfaces
 28 [15], membrane growth appears to be limited by the diffusion of one of the polyelectrolytes in the membrane on long
 29 time scales and membrane elasticity can be controlled with the concentration of polyelectrolytes [17, 21]. Monteillet
 30 *et al.* [18] studied the kinetics of assembly of polyelectrolytes at water-oil interfaces at macroscopic scales. They
 31 showed that the assembly was a two-stages process: a fast diffusion limited adsorption process which was followed by
 32 a much slower logarithmic process. The latter should result from the hindered interpenetration of the two oppositely
 33 charged polymers, such as coacervation in the bulk [22]. Moreover, self-consistent field analysis carried-out by the
 34 same group of authors suggested that the coacervate film should be heterogeneous [23]. This latter result highlights
 35 the importance of structural characterization at colloidal and macroscopic scales in order to describe the formation
 36 of membrane made of polyelectrolytes complex in relation with their structure and rheological properties. Moreover,
 37 given the difficulties associated with comparing the results, it is important to combine different methodologies using
 38 various interfacial characterization tools [24].

39 The aim of our work was to link the kinetics of the assembly of two oppositely charged polyelectrolytes at water-
 40 oil interface using a multiscale approach. In our study, chitosan, a water soluble cationic polymer, was used to form a
 41 complex with oil-soluble anionic phosphatidic acids at water-oil interface. This system has been used for microcapsule
 42 production [17, 21, 25]. However, its interest, for the present study, lies in the fact that the kinetics was relatively slow
 43 to study the different stage of the assembly of the polyelectrolytes. We characterized the kinetics of assembly at
 44 macroscopic scales by interfacial rheometer to follow the "gelation" of the interface with measurement of the velocity
 45 field of the interface. At colloidal scales, we developed space- and time- resolved dynamic light scattering (DLS) to
 46 characterize the changes in the heterogeneities of the interfaces, which was complemented by confocal and scanning
 47 electron microscopies (SEM). Lastly, this approach allowed us to relate the structure of the forming film with its
 48 rheological properties.

49 2. Materials and methods

50 2.1. Materials

51 Chitosan powder with medium molecular weight and 75-85% deacetylation was purchased from Sigma-Aldrich.
 52 The anionic surfactant used to complex the chitosan at water-oil interface was phosphatidic fatty acid (PFacid). It was
 53 comprised of a commercially available lecithin known as lecithin YN (Palsgaard 4448, food-grade, E442, Palsgaard).
 54 In mass, the phosphatidic acids were 55% w/w, neutral triglycerides 40% and ammonium salts 5%; see [17] for details.
 55 The molecular structures of both polyelectrolytes are given in Figure 2-A. Sodium hydroxide (1 mol/L) was purchased
 56 from VWR. The oil-soluble fluorescent dye, Hostasol Yellow 3G (HY-3G), was acquired from Clariant. Rapeseed
 57 oil (from *Brassica rapa*), hydrochloric acid (36.5-38.0 %, BioReagent, for molecular biology) and cyclohexane (anhy-
 58 drous, 99.5%) were obtained from Sigma-Aldrich. Deionized water (resistivity > 18 MΩ.cm) was produced from a

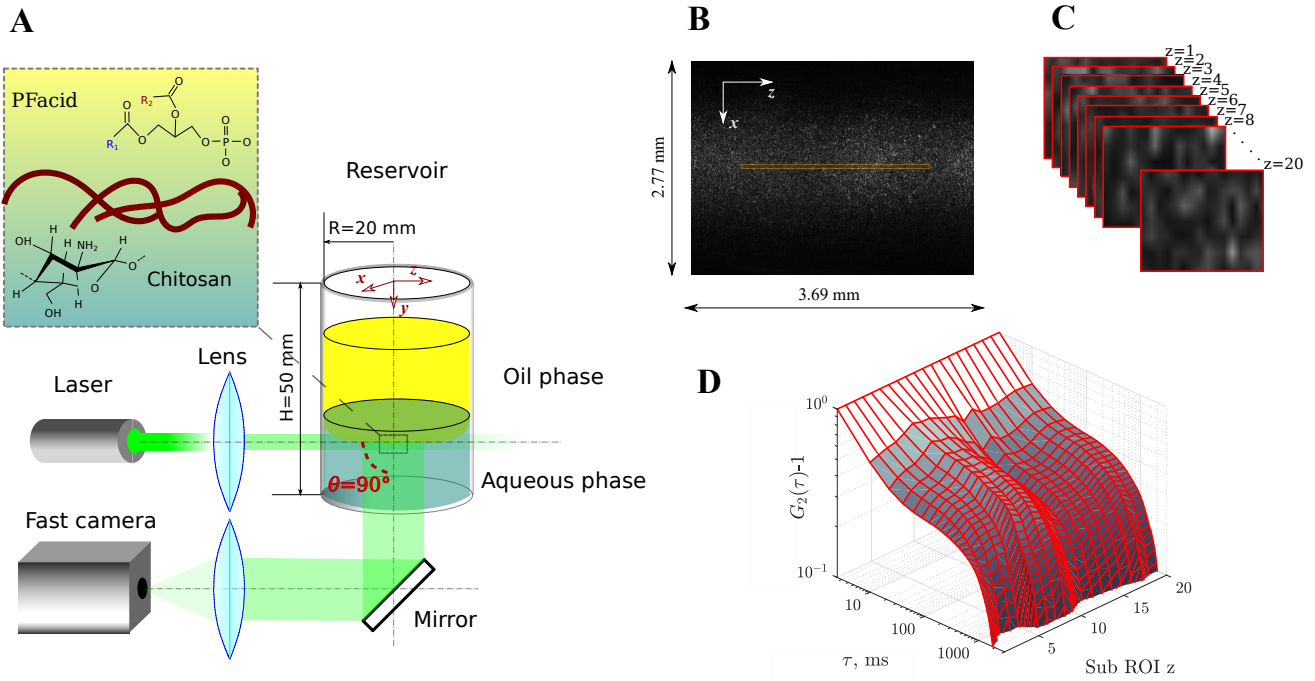


Figure 2: Representative sketch of multi-speckles Dynamic Light Scattering. (A) Chitosan / PFAcid membrane was formed at oil-water interface in a cylindrical container. The interface was illuminated by a laser beam set to propagate inside the membrane. The light scattered at 90° was reflected by a polarization holding mirror and collected with a lens onto the camera sensor. (B) Example of an image taken by the CCD camera. In the center, the laser illumination path is clearly visible, showing the speckles. The red rectangle in the middle shows the part of the image used for auto-correlation calculus. (C) Stack representation of the 20th sub-ROI obtained by sequencing the red rectangle in B in equisized small images. (D) Intensity correlation function $g_2 - 1$ as a function of the lag time τ and the sub-ROI z .

59 Millipore Filter water system. CellMask™ Deep Red Plasma membrane stain was obtained from ThermoFisher. All
 60 chemicals and solvents used in this study were commercially available and used as received unless stated otherwise.

61 The aqueous solution was obtained by dissolving chitosan powder in Millipore water and carefully adjusting the
 62 pH with hydrochloric acid (1 mol/L) at 3.0 to obtain a solution of 0.1 % w/w. The chitosan solution was then filtered to
 63 remove undissolved particles through Minisart syringe-filters (pore size 5.0 μm). The viscosity of the 0.1 % chitosan
 64 solution was 8 mPa·s.

65 The 1 % w/w stock solution of PFAcid was obtained by dissolving lecithin YN overnight in rapeseed oil (carefully
 66 stirred at 35°C). Undissolved particles were removed by centrifugation at $\times 1000g$ for one hour. The solution was
 67 the diluted with rapeseed oil to obtain a concentration of PFAcid ranging from 0.1 to 1 % w/w. The viscosity of these
 68 solutions was $62.6 \text{ mPa}\cdot\text{s}$ at $23 \pm 1^\circ\text{C}$.

69 2.2. Interfacial rheometry

70 An interfacial rheological study of a flat film of chitosan / PFAcid complex was performed with a bicone geometry
 71 using a commercially available solution (**Figure 1**), which is an appropriate approach for interfaces with high moduli
 72 and viscosities [26]. The Interfacial Rheology System (IRS, Anton Paar, Austria) was mounted on the Modular
 73 Compact Rheometer MCR 501 (Anton Paar, Austria) after being thoroughly washed with ethanol and Milli-Q water.
 74 For the interfacial measurements, the bicone geometry was positioned at the height $H_1 = 19.5 \text{ cm}$ from the bottom of
 75 the measuring cell after the zero-gap was established. Then the cell was filled with the aqueous phase until the normal
 76 force acting on the geometry was not adjusted to zero point in order to position the edge of the bicone geometry exactly
 77 at the interface. Next, the oil phase was gently added over the aqueous phase up to the total height $H = 40 \text{ cm}$. Every
 78 measurement was performed in 3-4 minutes after two phases were brought into contact. All oscillatory measurements
 79 were performed for at least five time periods per data point. All the measurements were conducted at room temperature
 80 ($23 \pm 1^\circ\text{C}$).

81 The interfacial viscoelastic properties of the chitosan / PFAcid membrane in oscillatory motion are described by

82 the frequency-dependant complex linear viscoelastic modulus G_i^* ,

$$G_i^*(\omega) = G_i'(\omega) + iG_i''(\omega) \quad (1)$$

83 where G_i' and G_i'' are the components of the interfacial complex modulus (two-dimensional elastic modulus and
84 loss modulus, respectively). It is related to the the complex interfacial viscosity η_i^* as [26]

$$G_i^*(\omega) = i\omega\eta_i^*(\omega) = -\omega\eta_i''(\omega) + i\omega\eta_i'(\omega) \quad (2)$$

85 where $\eta_i''(\omega)$ is the out-of-phase shear viscosity and $\eta_i'(\omega)$ is the the dynamic interfacial shear viscosity. The
86 contributions of the interfacial and bulk components to the torque appearing on the bicone geometry during its motion
87 were compared through the non-dimensional parameter, the Boussinesq number (Bo)

$$Bo(\omega) = \frac{\eta_i'(\omega) - i\eta_i''(\omega)}{a(\eta_b^{(1)} + \eta_b^{(2)})} \quad (3)$$

88 where η_b is the bulk viscosity (superscripts denote upper and lower fluid respectively) and a is the characteristic
89 length scale that depends on the measuring system. As usual, the interfacial flow was considered to be decoupled from
90 the bulk. In that case, the interfacial shear viscosity is calculated by [27]:

$$\eta = \frac{M - \frac{8}{3}R_2^3(\eta_b^{(1)} + \eta_b^{(2)})\Omega}{4\pi R_2^2\Omega} \quad (4)$$

91 where Ω is the angular velocity (Figure 1 A). This expression is only relevant for the $Bo \rightarrow \infty$. For low and
92 intermediate Bo a complete analysis must be used, since the influence of the bulk phases becomes important [27].
93 In our experiments the interfacial response was decoupled from the bulk one by using the Anton Paar application
94 software.

95 2.3. Particle tracking velocimetry

96 The displacements and velocity field on the oil-water interface during rheometric experiments were quantified
97 through particle tracking velocimetry (PTV). For this purpose, the water-oil interface was decorated at low coverage
98 with polyethylene microspheres (63-75 μm Cospheric LLC, USA) used as tracers. Less than 0.01% w/w of particle
99 powder was added to 100 ml of oil phase and mixed thoroughly with a magnetic stirrer overnight. This volume of
100 oil containing tracers was further used for rheological experiments as described above in the Section 2.2. The USB
101 microscope (A1 USB Digital Microscope, Andonstar) was immersed in the oil phase during rheological experiments
102 in IRS in order to visualize the displacement of microspheres under the shear flow. The image sequences were recorded
103 at 20 frames per second and post-processed with a custom written particle tracking routine (MATLAB, MathWorks).

104 2.4. Dynamic light scattering

105 The dynamic evolution of the structure of the membrane was measured by space resolved Dynamic Light Scattering
106 (DLS) at constant temperature $T=22^\circ\text{C}$. A sketch of the custom-built DLS set-up is shown in Figure 2. The oil-
107 water interface, which later became a membrane, was illuminated by a vertically polarized laser beam produced by a
108 single-mode laser (MSLIII, CNI, China, $\lambda = 532 \text{ nm}$). The laser beam had a diameter of 2 mm and was shaped by
109 a combination of two lenses with focal lengths $f_1 = 200 \text{ mm}$ and $f_2 = 25.4 \text{ mm}$. The coherent light was scattered
110 by forming solid matter at the oil-water interface. Only the light scattered at 90° was collected, after reflection onto
111 a non-polarized mirror. Focusing the laser beam on the interface was a complicated technical task, as the oil-water
112 interface formed a concave-convex meniscus depending on the wettability of the cylinder. However the chitosan/PFacid
113 complexation leading to the membrane formation resulted in a drastic decline in interfacial tension causing the interface
114 to flatten. This led to the interface displacement along y-axis and consequently signal loss. In order to minimise this
115 effect, all measurements were performed using a large custom-made glass cylindrical container positioned vertically

116 and sealed underneath with a flat sheet of glass. The dimensions of the reservoir rendered the interface displacement
 117 negligible and the precise control of the sample volume ensured the tangential contact between the interface and the
 118 laser beam throughout the experiments.

119 In order to follow the structural evolution of the membrane, the scattered intensity was collected either with a CCD
 120 camera (acA640-100gm, Basler, Germany) or with a photomultiplier (SPCM-AQR-13, excelitas Technologies, USA).
 121 When the camera was used, a lens with a focal length $f_l = 150$ mm allowed the image of the scattering volume to
 122 form onto the CCD sensor. A diaphragm placed in the focal plane of the lens was set in order to optimize the size of
 123 the speckles to the pixel size of the camera [28]. For fast processes, the photomultiplier associated with a correlator
 124 (Flex03-LQ, Correlator.com, USA) was used to widen the dynamic range of acquisition to include lag times as small
 125 as 10^{-6} s.

126 Our approach enabled nondestructive probing of the interfacial membrane evolution with both spacial and temporal
 127 resolution, as long as the characteristic relaxation time of the studied system allows signal detection with a digital
 128 camera. The scattered light detected by CCD camera created the image of a coherence area known as speckle (Figure
 129 2 B). The red rectangle in the center of the image represents the Region Of Interest (ROI), only this part of the image
 130 has been used for analysis. This area was sequenced into 20 sub-ROI (Figure 2 C). The individual time autocorrelation
 131 function of the scattered intensity $g_2(\tau) - 1$ was computed for each sub-ROI

$$g_2(\tau, z) - 1 = \frac{\langle I^z(t)I^z(t + \tau) \rangle_t}{\langle I^z(t)^2 \rangle_t} - 1 \quad (5)$$

132 where $I^z(t)$ is the intensity collected within z^{th} sub-ROI and $\langle \dots \rangle_t$ denotes averaging over time. Figure 2 D shows
 133 the result of the intensity correlation function as a function of the sub-ROI z and the lag time τ .

134 We also used the Time Resolved Correlation scheme (TRC) which allows DLS investigation of heterogeneous
 135 dynamics, as introduced by [29, 30, 31]. Analogously to $g_2(\tau) - 1$, the correlation degree $c_I(t, \tau, z)$ was calculated
 136 individually for each sub-ROI

$$c_I(t, \tau, z) = \frac{\langle I_p^z(t)I_p^z(t + \tau) \rangle_p}{\langle I_p^z(t) \rangle_p \langle I_p^z(t + \tau) \rangle_p} - 1 \quad (6)$$

137 where $I_p^z(t)$ is the intensity measured at time t for the p^{th} pixel of an image within z^{th} sub-ROI and $\langle \dots \rangle_p$ denotes
 138 averaging over pixels.

139 2.5. Microscopy

140 Scanning electron microscopy (SEM) was used to characterize the morphology of chitosan / PFAcid membrane at
 141 short complexation time. The membranes were grown on the surface of chitosan drops suspended in oil phase which
 142 contained PFAcid. Once the required complexation time was achieved the droplets were washed in large quantities
 143 cyclohexane (for more details see [17], [21]) in order to remove the oil with the residues of anionic surfactant. The
 144 chitosan droplets encapsulated with the membrane were placed on a cover slip and dried at room temperature. Dried
 145 chitosan / PFAcid membrane were observed by scanning electron microscopy (SEM). Samples were coated with Au/Pd
 146 in a Baltec MED-020 sputter coater and observed in secondary electron mode in a Thermo Scientific Quanta 250
 147 microscope equipped with a field emission gun and operating at 2.5 kV.

148 Confocal microscopy was used to characterize the morphology of chitosan / PFAcid membrane at long complexation
 149 time. Analogously to the SEM characterization described above, the chitosan droplets were injected into oil phase
 150 containing anionic surfactant. Wet (no cyclohexane washing) chitosan / PFAcid membrane were observed with Leica
 151 TCS SP8 scanning point confocal microscope equipped with a $\times 63$ water immersion objective and in-plane image
 152 resolution $0.36 \mu\text{m}/\text{px}$.

153 3. Results and discussion

154 3.1. Interfacial rheology of chitosan / PFAcid membrane

155 We analysed the kinetics of formation of the membrane with a time sweep experiment at constant amplitude ($\dot{\gamma} =$
 156 0.03%) and frequency ($f = 0.5$ Hz). The choice of these parameters was justified by the need to keep the deformation

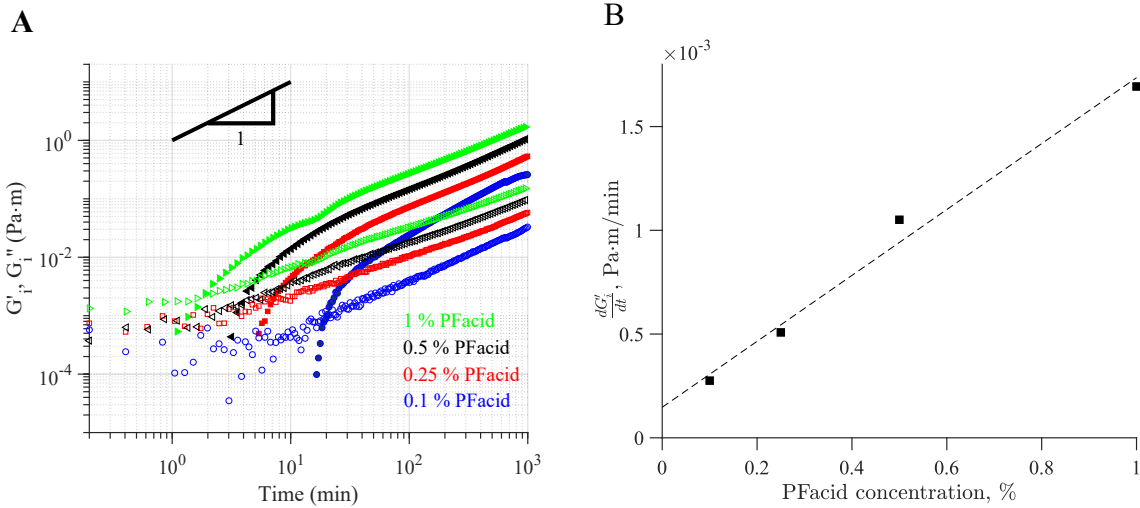


Figure 3: Macroscopic study of the interfacial rheological properties of a chitosan / PFacid membrane. (A) Typical time-dependant evolution of interfacial elastic G'_i and viscous G''_i shear moduli at different concentrations of PFacid. $f = 0.5$ Hz, $\dot{\gamma} = 0.03\%$ Chitosan 0.1% w/w (B) Following a long-term linear regime of membrane, the growth rate of interfacial elastic modulus G'_i , as a function of anionic surfactant concentration roughly follows a linear law.

157 within the linear viscoelastic regime while maintaining the torque as high as possible (see Figure SI 1). However, as
 158 explained below, the kinetics depended on the applied strain. Figure 3-A depicts the evolution of G'_i and G''_i over time
 159 for different concentrations of PFacid. As a control, a pure water-oil interface without membrane formation was also
 160 quantified (see Figure SI 2), which showed a constant G''_i of $\sim 10^{-3}$ N/m whereas G'_i was null. In the early stage of
 161 membrane formation ($t < 1$ min for 1% w/w PFacid and 10 min for 0.1% w/w PFacid), G''_i was almost constant and
 162 close to the system without PFacid. G'_i was out of the measurement sensitivity. In this regime, the interface manifested
 163 purely liquid-like properties. However, within a few minutes, a slow increment in G''_i was accompanied by a rapid
 164 growth of G'_i . The interfacial storage modulus G'_i quickly overcame G''_i , manifesting the prevalence of solid-like
 165 properties. After ten hours of complexation, both interfacial moduli increased on a roughly linearly basis. The atomic
 166 force microscopy measurements (see **Supporting material**) indicate that the chitosan/PFacid film thickness scales
 167 with time as $\sim t^{0.5}$. Considering that the long term linear development of the interfacial moduli suggests a nonlinear
 168 relation between interfacial moduli and the membrane thickness.

169 The time for which the interfacial elasticity G''_i growth abruptly, increased with the concentration of PFacid, Figure
 170 3-A. Following the initial rapid transition, the growth rate of G'_i slowed down and increased linearly over time. The
 171 growth rate of interfacial elastic modulus also scaled on a linear basis with the concentration of PFacid, Figure 3-B.

172 To gain insight into the mechanisms at play in the early moments of membrane formation, creep experiments on the
 173 forming membrane were coupled to visualisation of the deformation of the interface by PTV (Figure 4). In these creep
 174 experiments, the bicone geometry was put into motion at fixed torque values and the deformation was measured. As the
 175 membrane was forming, the shear strain increased gradually until the geometry was brought to arrest. The evolution
 176 of the deformation varied with the applied torque, Figure 4-A. In analogy with percolation of particle laden interfaces
 177 [10], we termed the time at which the strain rate was null, the percolation time. The percolation time increased on a
 178 roughly a linear basis with the applied torque, Figure 4-B. Thus, the percolation process of the interface was coupled
 179 to the interfacial shear rate. The water-oil interface was decorated at low coverage with polyethylene microspheres (\sim
 180 $70 \mu\text{m}$) used as tracing particles. The radial velocity profile v of the interface was parabolic during the first few minutes
 181 of reaction, as expected for liquid interfaces. The spatio-temporal evolution of the velocity shows that the geometry
 182 slow-down was associated with the flattening of the velocity profile, Figure 4-C,D. Macroscopically, we observed
 183 that the shear rate tended towards zero in regions closed from the geometry ($r = 0$ and R). However, the velocity
 184 distribution was strongly heterogeneous before the arrest of the geometry. In fact, a closer look at the interface showed
 185 a constant formation and rupture of the membrane. We observed small patch-like sheet membranes that grew all over
 186 the interface and accumulated close to the geometry (see **Supporting video**). When the amount of membrane pieces
 187 was high enough to fully cover the interface, the interface jammed and stopped the motion of the geometry. This result
 188 fitted with non-reactive particle laden-interface for which domains of packed particles create elastic interfaces. When

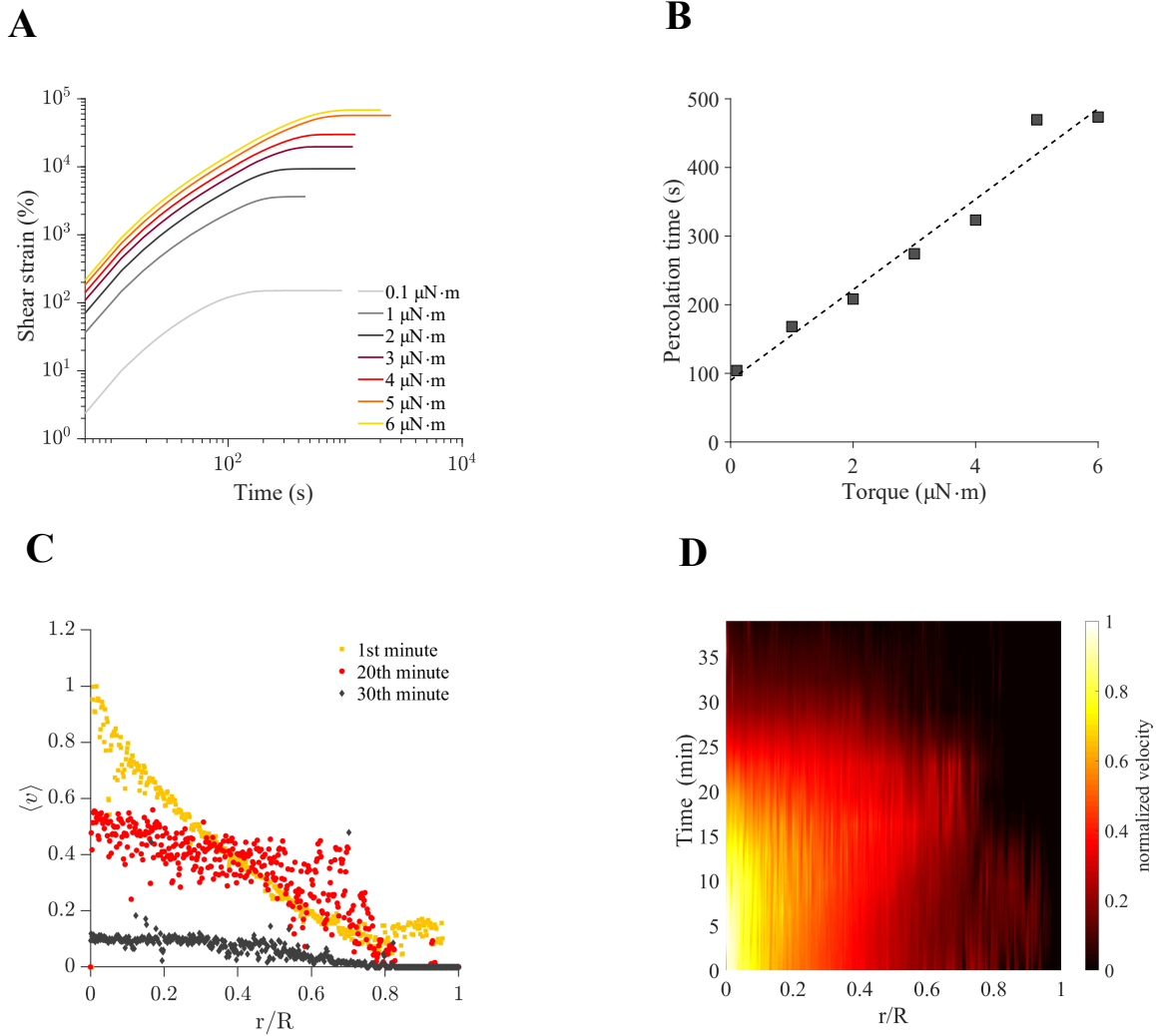


Figure 4: Particle tracking on the water-oil interface during the creep experiment. (A) Creep experiments at the water-oil interface during the membrane formation at different torque values. (B) The time required to stop the rotation of the geometry increased on a roughly linear basis with the torque. (C) Normalized velocity profiles at the interface at different stages of membrane formation. (D) The heatmap of normalized velocity values at the different points in time.

189 these domains start to break-up, a transition to viscous-like behavior was observed [32]. Finally, we concluded that
 190 the complexation of chitosan with PFAcid is a two-step process. At short time scale, the interface has a macroscopic
 191 rheological behaviour which is characteristic of liquid interfaces, but the interface is strongly heterogeneous and is
 192 composed of solid patches. At a critical time, called the percolation time, the patches pave the interface and percolated,
 193 which is macroscopically characterized by a sudden increase of the interfacial elastic modulus G'_i . At long time scales,
 194 the thickness of the membrane grew, as G'_i increased, by diffusion of one of the polyelectrolytes inside the membrane
 195 [15, 17].

196 3.2. Dynamic light scattering experiments

197 In order to shed light on the structural evolution of the interface formation, we employed DLS and TRC analysis
 198 [29, 30, 33], see Figure 2 for the experimental set-up. The interface was formed at the water-oil interface in a cylindrical
 199 reservoir via complexation between 0.1% w/w chitosan and 1% w/w PFAcid, Figure 2. During the first 2 s, $C_I(\tau = 0, t)$
 200 fluctuated randomly around a steady value of $\approx 10^{-2}$, Figure 5. Such behaviour corresponds to a Brownian system
 201 [29, 31], meaning that the displacement of particles between any two frames was on average the same, independently
 202 of the complexation time t . Beyond 2 s, the resolved correlation function drastically increased and gained half a decade
 203 in 100 s, meaning that the degree of correlation in the sample increased. This behaviour indicated the formation of a

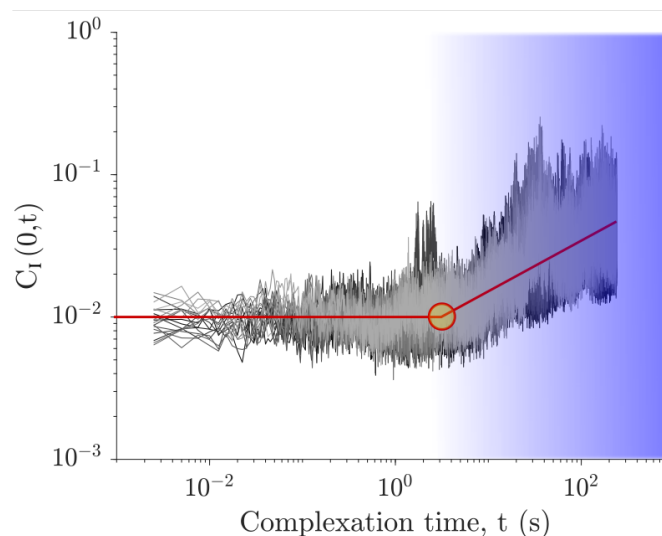


Figure 5: Time Resolved Correlation (TRC) at 0 lag time (τ) of building interface of the 20 ROIs. Straights lines are eye-guides and the circle at line interception indicates the starting time of the membrane gelation.

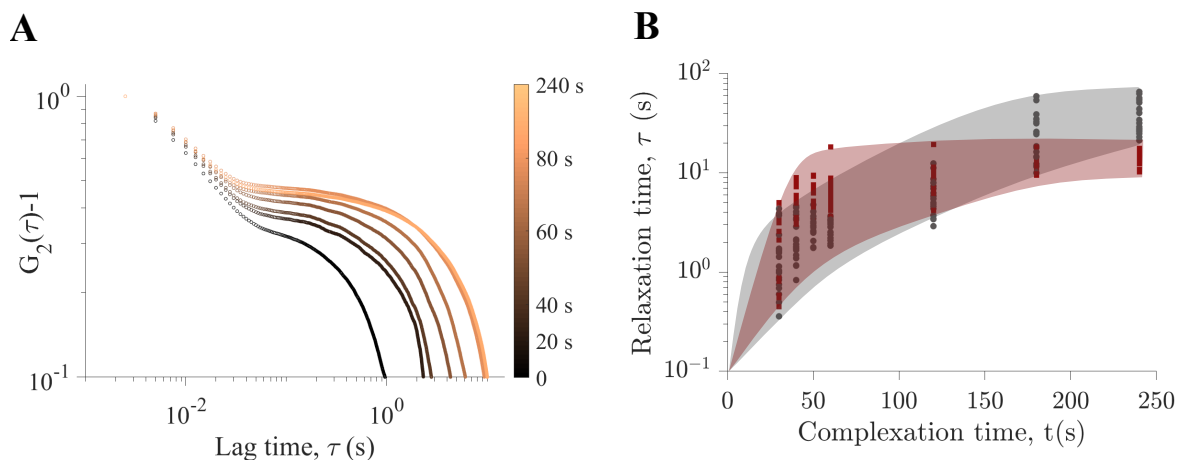


Figure 6: (A) Auto-correlation function of the interface computed from the mean time of TRC as at different lag times for an ROI as a function of the time from 0 to 240 s. (B) Evolution of the relaxation times of the forming interface within different sub-ROI computed for two separate experiments at identical conditions. The colored areas separating two experiments serve as guiding lines

204 gel-like interface [29], the result similar to that obtained in rheological study.

205 The kinetics of membrane formation was also probed with the intensity correlation function $G_2(\tau) - 1$. Figure 6-A
 206 shows the intensity correlation function computed at different lag times following the formation time of the membrane
 207 from 0 to 240 s. At 0 s, the intensity correlation function was identical to the correlation of the chitosan alone (see
 208 **Supporting material**) with a relaxation time of 0.1 s. As the time increased, a second relaxation time appeared as
 209 a second mono-exponential function for which relaxation time increased from 0.1 s to more than 10 s in 200 s of mem-
 210 brane complexation. After long complexation (10 hours), the characteristic relaxation time of a membrane increased
 211 up to 2×10^3 (see **Supporting material**).

212 More interestingly, DLS measurements were also resolved in space, which gave us insight into the formation of
 213 patches observed during rheological characterisation. The results of spatial analysis are depicted in Figure 6-B, where
 214 each dot corresponds to an ROI of $56 \mu\text{m} \times 56 \mu\text{m}$. Initially, the relaxation time at the interface was the same as that
 215 of the chitosan. As the chitosan / PFacid complexation took place and a solid matter started to appear at the interface,
 216 the relaxation time increased. At the different complexation times considered here, the relaxation times differed by
 217 nearly one decade between different ROI. It indicated high dynamic heterogeneity in the interface complexation. This

218 was consistent with the observation of patches during the interfacial rheological measurement. We concluded that
219 interfacial complexation of both polyelectrolytes is a spatially heterogeneous process.

220 3.3. Scanning electron and confocal microscopy

221 The morphology of chitosan / PFacid membranes formed at relatively short time scales was observed by Scanning
222 electron microscopy (SEM). In order to minimise harsh manipulations with fragile membranes, chitosan / PFacid
223 membranes were grown on a surface of water droplets in oil phase containing chitosan and PFacid respectively, for
224 more details see [21]. The complexation reaction was stopped by a gentle washing in large quantities of cyclohexane.
225 After that, the droplets now enclosed by a solid membrane were placed on the glass substrate and dried prior the SEM
226 imaging.

227 Figure 7 demonstrates the morphology of the chitosan / PFacid formed at 0.5 and 2 min of complexation time.
228 The short time formed membrane was characterized by an important heterogeneity of its structure (Figure 7 A). The
229 membrane appeared to be formed out of a large number of non-connected patches of 1-5 μm . Additionally, large non-
230 circular holes up to 10 μm were found in the membrane. At 2 minutes of complexation the interface appeared to be
231 fully formed, except for the presence of large circular holes (Figure 7 B). Figure 7 C shows the transversal view of the
232 membrane, which was characterized by sub-micrometric aggregates.

233 The confocal imaging was carried out on the thick membrane after 48h of complexation in order to reveal the
234 internal structure of the interface. Water droplets containing 0.1 % w/w concentration of chitosan were injected into
235 the oil phase containing 0.1 % w/w concentration of PFacid. Water-soluble fluorescent dye with high lipid affinity
236 (CellMask™ Deep Red plasma membrane stain, Invitrogen™) was added to the aqueous phase. This dye has little to
237 no fluorescence in a free form and is only fluorescent once it is "anchored" to lipids. Figure 7 depicts the results of
238 confocal imaging. These images show that the membrane was composed of nano-metric inclusions. Figure 7-right
239 shows the concentration gradient of these inclusions from the oil phase towards the aqueous phase. As the fluorescent
240 dye anchored to lipids, we deduced that this gradient of light intensity corresponds to a gradient of PFacid.

241 This set of microscopy images consolidated the idea that membrane formation was due to the percolation of in-
242 dividual patches. When the patches were able to form a percolated network, large holes were present. These results
243 were reminiscent of interfaces covered by model nanoparticles which form heterogeneous structures with voids for
244 low particle surface coverage [12, 11, 10]. The basic bricks are sub-micrometric aggregates of polyelectrolytes. On
245 long time scales, the membrane was fully covered of these aggregates. In the thickness of the membrane, there was a
246 negative gradient of these aggregates from the oil phase to the water phase. This last result supports the idea that the
247 growth of the membrane was limited by the diffusion through a gel-like porous network of PFacid on long time scales,
248 as described for H-bond donor / acceptor polymers [15].

249 4. Conclusion

250 Membrane formation based on the complexation between chitosan and short chain fatty acid has been used as
251 a model for interfacial self-assembly of poly-electrolytes. A multi-scale approach was used in order to perform a
252 characterisation of membrane formation and morphology.

253 The rheological properties of the forming membrane at macroscopic scale were probed by a combination of inter-
254 facial rheometry using the bicone geometry and particle tracking velocimetry of the interface. On short time scales, the
255 interface had a fluid-like behaviour and was composed of non-connected solid patches. The elastic behaviour emerged
256 when the patches percolated, similarly to a particle laden interface with an increasing surface coverage [13, 12, 10].
257 On long time scales, the surface elasticity increased almost linearly with time and concentration of the short chain fatty
258 acid. This regime was reminiscent of a membrane growth limited by the diffusion of the smallest entity of both com-
259 plexing molecules, as observed for polymer membranes obtained by h-bonding [9, 14, 15]. This finding was supported
260 by confocal imaging showing a concentration gradient of short chain fatty acid through the membrane.

261 The membrane formation is a two step process. First the interfacial reaction takes place and is governed by the
262 reactivity of the interacting species. Then the reaction takes place in the membrane and is limited by the diffusion
263 through the interfacial membrane. We employed several techniques in order to characterize these processes at different
264 scales. At microscopic scales, we characterized the structure of the interface by space- and time- resolved DLS, used
265 up to now in bulk for gels [33, 31, 29]. The method demonstrated that membrane formation was strongly heterogeneous
266 in space and confirmed that was a two step process. On short time-scale, the speckles were strongly non-correlated,
267 meaning that the interface had a fluid-like behaviour. On long time scales, the correlation of the speckles increased,

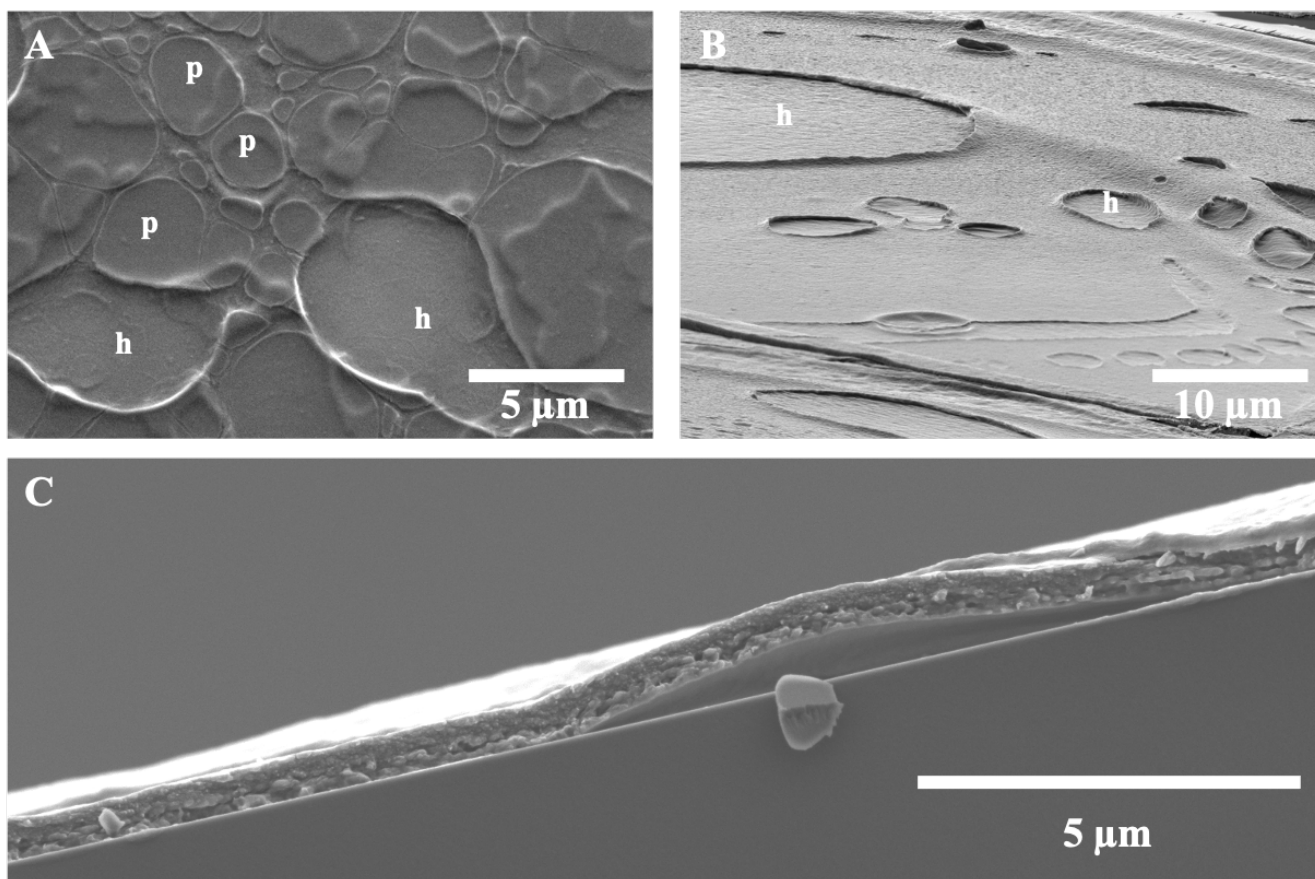


Figure 7: SEM images of dried chitosan / PFacid membrane. (A) CH / PFacid membrane after 30 s of complexation. The interface was made of individual patches of 1-50 μm size (p), as well as large holes (h). (B) CH / PFacid membrane after 2 min of complexation. The interface was homogeneous, with the exception of circular holes (h). (C) View in the thickness of the membrane after 2 min of complexation. The membrane showed a granular structure.

268 as a sign of the gelation of the interface. The strong spatial heterogeneity was consistent with a process of membrane
 269 growth due to the formation of nuclei and then their percolation to form a gel. The employed method allows the
 270 dynamic and non-destructive measurement of the forming film without stopping the reaction.

271 Some of the other types of interfacial polymerization reactions that proved to be very interesting for industrial
 272 applications (such as polyamide, polyurethane, polyurea and etc. membranes) were studied extensively [34]. For these
 273 reaction types the membrane growth was confirmed to take place in organic phase. We however observed the smaller
 274 anionic surfactant to diffuse through the membrane into the aqueous phase. SEM and confocal imaging confirmed
 275 the presence of microscopic patches and showed also that the basic bricks were sub-micrometric aggregates of poly-
 276 electrolytes. When the interface was fully covered with these aggregates, the membrane grew in its thickness by a
 277 diffusion-like process of the short chain fatty acid. This finding was supported by the growth of the elastic modulus
 278 with the concentration of PFacid and the gradient of PFacid in the thickness of the membrane.

279 Finally, this multi-scale experimental approach created a robust overarching picture of the interfacial complexation
 280 of polyelectrolytes. At short time scales, the growth is limited by the formation of "nuclei" which form patches. This
 281 work brings new elements on interfacial complexation that should prove useful to control the properties of liquid-liquid
 282 interfaces for the design of new materials, such as microcapsules or structured liquids.

283 5. Acknowledgements

284 LRP is part of the LabEx Tec21 (ANR-11-LABX-0030) and of the PolyNat Carnot Institute (ANR-11-CARN-007-
 285 01). The authors express their sincere gratitude to Christine Lancelon-Pin (CERMAV-CNRS, Grenoble, France) for
 286 her assistance with scanning-electron microscopy. The authors acknowledge the NanoBio-ICMG chemistry platform

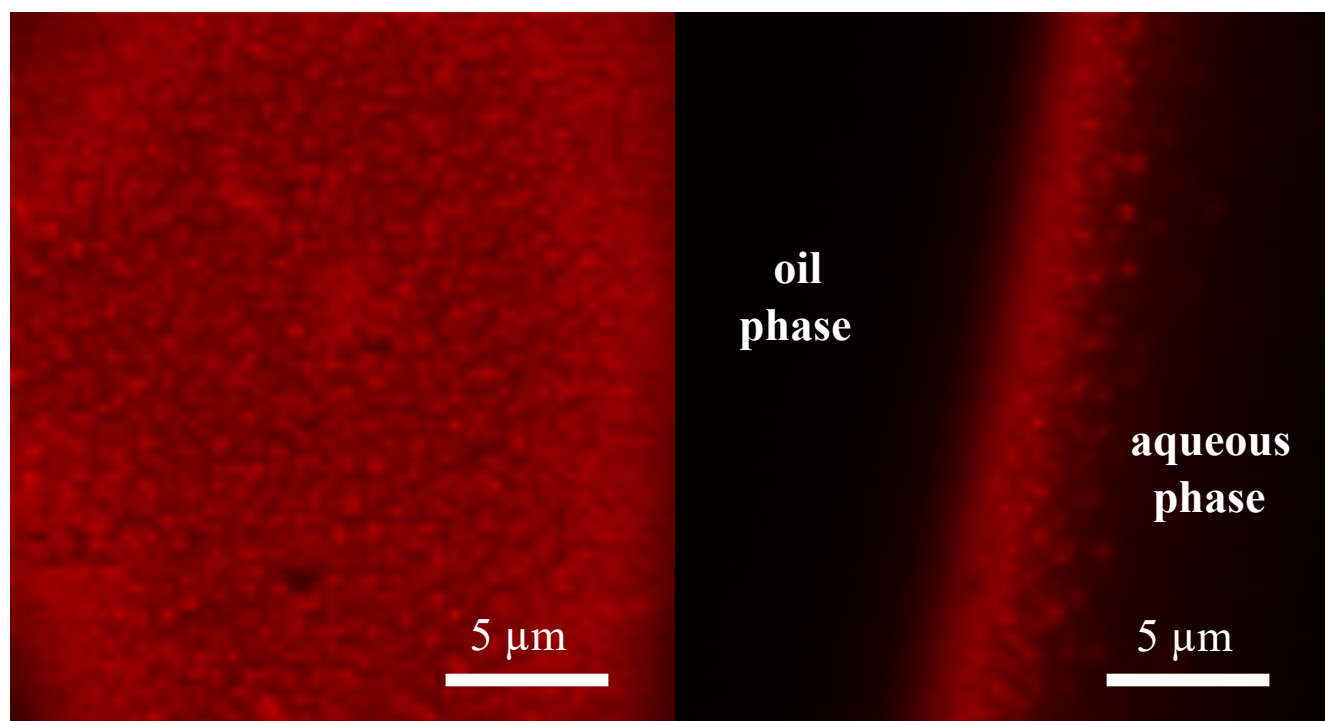


Figure 8: Confocal images of wet Chitosan / PFacid membrane after 48h of complexation. The membrane was marked by a fluorescent dye with lipid affinity (see text for details). Left: A piece of a membrane laying flat on a glass substrate showing a granularly patterned structure. Right: A horizontal confocal slice of a labeled membrane.

287 (UAR 2607, Grenoble) for granting access to the electron microscopy facilities. The authors thank the support of ANR
 288 2DVisc (ANR-18-CE06-0008-01).

289 6. Author contributions

290 **Revaz Chachanidze:** Conceptualization, Methodology, Formal analysis, Investigation, Writing - Original Draft,
 291 Visualization **Kailie Xie:** Conceptualization, Methodology, Investigation, Writing - Review & Editing **Hanna Mas-**
 292 **sad:** Methodology, Formal analysis, Investigation, Writing - Original Draft, Visualization **Denis Roux:** Methodology,
 293 Formal analysis, Writing - Original Draft, Supervision **Marc Leonetti:** Conceptualization, Methodology, Writing -
 294 Original Draft, Supervision **Clément de Loubens:** Conceptualization, Methodology, Writing - Original Draft, Super-
 295 vision

296 References

- 297 [1] W. Ramsden, Separation of solids in the surface-layers of solutions and ‘suspensions’ (observations on surface-membranes, bubbles, emulsions,
 298 and mechanical coagulation).—preliminary account, Proceedings of the royal Society of London 72 (477-486) (1904) 156–164.
 299 [2] S. U. Pickering, Cxciv.—the interaction of metallic sulphates and caustic alkalis, Journal of the Chemical Society, Transactions 91 (1907)
 300 1981–1988.
 301 [3] J. Forth, P. Y. Kim, G. Xie, X. Liu, B. A. Helms, T. P. Russell, Building reconfigurable devices using complex liquid–fluid interfaces, Advanced
 302 Materials 31 (18) (2019) 1806370.
 303 [4] P. Bertsch, J. Bergfreund, E. J. Windhab, P. Fischer, Physiological fluid interfaces: Functional microenvironments, drug delivery targets, and
 304 first line of defense, Acta Biomaterialia (2021).
 305 [5] E. Amstad, Capsules: Their past and opportunities for their future (2017).
 306 [6] R. Xu, T. Liu, H. Sun, B. Wang, S. Shi, T. P. Russell, Interfacial assembly and jamming of polyelectrolyte surfactants: A simple route to print
 307 liquids in low-viscosity solution, ACS Applied Materials & Interfaces 12 (15) (2020) 18116–18122.
 308 [7] A. Maestro, Tailoring the interfacial assembly of colloidal particles by engineering the mechanical properties of the interface, Current opinion
 309 in colloid & interface science 39 (2019) 232–250.
 310 [8] J. N. Israelachvili, Intermolecular and surface forces, Academic press, 2015.
 311 [9] J. D. de Baubigny, C. Trégouët, T. Salez, N. Pantoustier, P. Perrin, M. Reyssat, C. Monteux, One-step fabrication of ph-responsive membranes
 312 and microcapsules through interfacial h-bond polymer complexation, Scientific reports 7 (1) (2017) 1–7.

- 313 [10] J. H. Thijssen, J. Vermant, Interfacial rheology of model particles at liquid interfaces and its relation to (bicontinuous) pickering emulsions,
314 Journal of Physics: Condensed Matter 30 (2) (2018) 023002.
- 315 [11] S. Reynaert, P. Moldenaers, J. Vermant, Interfacial rheology of stable and weakly aggregated two-dimensional suspensions, Physical Chemistry
316 Chemical Physics 9 (48) (2007) 6463–6475.
- 317 [12] K. Masschaele, J. Franssaer, J. Vermant, Direct visualization of yielding in model two-dimensional colloidal gels subjected to shear flow,
318 Journal of rheology 53 (6) (2009) 1437–1460.
- 319 [13] M. Cui, T. Emrick, T. P. Russell, Stabilizing liquid drops in nonequilibrium shapes by the interfacial jamming of nanoparticles, Science
320 342 (6157) (2013) 460–463.
- 321 [14] S. Le Tirilly, C. Tregouët, S. Bône, C. Geffroy, G. Fuller, N. Pantoustier, P. Perrin, C. Monteux, Interplay of hydrogen bonding and hydrophobic
322 interactions to control the mechanical properties of polymer multilayers at the oil–water interface, ACS Macro Letters 4 (1) (2015) 25–29.
- 323 [15] J. Dupré de Baubigny, P. Perrin, N. Pantoustier, T. Salez, M. Reyssat, C. Monteux, Growth mechanism of polymer membranes obtained by
324 h-bonding across immiscible liquid interfaces, ACS Macro Letters 10 (2) (2021) 204–209.
- 325 [16] D. Grigoriev, T. Bukreeva, H. Möhwald, D. Shchukin, New method for fabrication of loaded micro- and nanocontainers: emulsion encapsulation
326 by polyelectrolyte layer-by-layer deposition on the liquid core, Langmuir 24 (3) (2008) 999–1004.
- 327 [17] D. Z. Gunes, M. Pouzot, M. Rouvet, S. Ulrich, R. Mezzenga, Tuneable thickness barriers for composite o/w and w/o capsules, films, and their
328 decoration with particles, Soft Matter 7 (19) (2011) 9206–9215.
- 329 [18] H. Monteillet, F. Hagemans, J. Sprakel, Charge-driven co-assembly of polyelectrolytes across oil–water interfaces, Soft Matter 9 (47) (2013)
330 11270–11275.
- 331 [19] G. Kaufman, R. Boltyskiy, S. Nejadi, A. R. Thiam, M. Loewenberg, E. R. Dufresne, C. O. Osuji, Single-step microfluidic fabrication of soft
332 monodisperse polyelectrolyte microcapsules by interfacial complexation, Lab on a Chip 14 (18) (2014) 3494–3497.
- 333 [20] M. Kim, S. J. Yeo, C. B. Highley, J. A. Burdick, P. J. Yoo, J. Doh, D. Lee, One-step generation of multifunctional polyelectrolyte microcapsules
334 via nanoscale interfacial complexation in emulsion (nice), ACS nano 9 (8) (2015) 8269–8278.
- 335 [21] K. Xie, C. de Loubens, F. Dubreuil, D. Z. Gunes, M. Jaeger, M. Leonetti, Interfacial rheological properties of self-assembling biopolymer
336 microcapsules, Soft matter 13 (36) (2017) 6208–6217.
- 337 [22] E. Spruijt, J. Sprakel, M. Lemmers, M. A. C. Stuart, J. van der Gucht, Relaxation dynamics at different time scales in electrostatic complexes:
338 Time-salt superposition, Phys. Rev. Lett. 105 (2010) 208301. doi:10.1103/PhysRevLett.105.208301.
339 URL <https://link.aps.org/doi/10.1103/PhysRevLett.105.208301>
- 340 [23] H. Monteillet, J. Kleijn, J. Sprakel, F. Leermakers, Complex coacervates formed across liquid interfaces: A self-consistent field analysis,
341 Advances in colloid and interface science 239 (2017) 17–30.
- 342 [24] M. D. Biviano, L. J. Böni, J. D. Berry, P. Fischer, R. R. Dagastine, Viscoelastic characterization of the crosslinking of β -lactoglobulin on
343 emulsion drops via microcapsule compression and interfacial dilational and shear rheology, Journal of Colloid and Interface Science 583
344 (2021) 404–413.
- 345 [25] M. Maleki, C. de Loubens, K. Xie, E. Talansier, H. Bodiguel, M. Leonetti, Membrane emulsification for the production of suspensions of
346 uniform microcapsules with tunable mechanical properties, Chemical Engineering Science 237 (2021) 116567.
- 347 [26] D. Renggli, A. Aliche, R. H. Ewoldt, J. Vermant, Operating windows for oscillatory interfacial shear rheology, Journal of Rheology 64 (1)
348 (2020) 141–160.
- 349 [27] P. Erni, P. Fischer, E. J. Windhab, V. Kusnezov, H. Stettin, J. Läger, Stress- and strain-controlled measurements of interfacial shear viscosity
350 and viscoelasticity at liquid/liquid and gas/liquid interfaces, Review of Scientific Instruments 74 (11) (2003) 4916–4924. arXiv:<https://doi.org/10.1063/1.1614433>, doi:10.1063/1.1614433.
351 URL <https://doi.org/10.1063/1.1614433>
- 352 [28] N. Ali, Rhéospeckle : un nouvel outil d'étude du comportement multi-échelle des matériaux hétérogènes, Ph.D. thesis, Université Grenoble
353 Alpes, thèse de doctorat dirigée par Roux, Denis et Caton, François (2016).
354 URL <http://www.theses.fr/2016GREAI013>
- 355 [29] L. Cipelletti, H. Bissig, V. Trappe, P. Ballesta, S. Mazoyer, Time-resolved correlation: a new tool for studying temporally heterogeneous
356 dynamics, Journal of Physics: Condensed Matter 15 (1) (2002) S257.
- 357 [30] H. Bissig, S. Romer, L. Cipelletti, V. Trappe, P. Schurtenberger, Intermittent dynamics and hyper-aging in dense colloidal gels, PhysChem-
358 Comm 6 (5) (2003) 21–23.
- 359 [31] A. Duri, H. Bissig, V. Trappe, L. Cipelletti, Time-resolved-correlation measurements of temporally heterogeneous dynamics, Phys. Rev. E 72
360 (2005) 051401. doi:10.1103/PhysRevE.72.051401.
361 URL <https://link.aps.org/doi/10.1103/PhysRevE.72.051401>
- 362 [32] S. Barman, G. F. Christopher, Role of capillarity and microstructure on interfacial viscoelasticity of particle laden interfaces, Journal of
363 Rheology 60 (1) (2016) 35–45.
- 364 [33] E. Secchi, T. Roversi, S. Buzzaccaro, L. Piazza, R. Piazza, Biopolymer gels with “physical” cross-links: gelation kinetics, aging, heterogeneous
365 dynamics, and macroscopic mechanical properties, Soft Matter 9 (15) (2013) 3931–3944.
- 366 [34] C. Perignon, G. Ongmayeb, R. Neufeld, Y. Frere, D. Poncelet, Microencapsulation by interfacial polymerisation: Membrane formation and
367 structure, Journal of microencapsulation 32 (2014) 1–15. doi:10.3109/02652048.2014.950711.
- 368